High-Performance Flexible Broadband Photodetector Based on Organolead Halide Perovskite

Xin Hu, Xiaodong Zhang, Lin Liang, Jian Bao, Shuang Li, Wenlong Yang, and Yi Xie**

Organolead halide perovskites have attracted extensive attentions as light harvesting materials for solar cells recently, because of its high charge-carrier mobilities, high photoconversion efficiencies, low energy cost, ease of deposition, and so on. Herein, with $CH_3NH_3PbI_3$ film deposited on flexible ITO coated substrate, the first organolead halide perovskite based broadband photodetector is demonstrated. The organolead halide perovskite photodetector is sensitive to a broadband wavelength from the ultraviolet light to entire visible light, showing a photo-responsivity of 3.49 A W^{-1}, 0.0367 A W^{-1}, an external quantum efficiency of 1.19×10^3%, 5.84% at 365 nm and 780 nm with a voltage bias of 3 V, respectively. Additionally, the as-fabricated photodetector exhibit excellent flexibility and robustness with no obvious variation of photocurrent after bending for several times. The organolead halide perovskite photodetector with high sensitivity, high speed and broad spectrum photoresponse is promising for further practical applications. And this platform creates new opportunities for the development of low-cost, solution-processed and high-efficiency photodetectors.

1. Introduction

The photodetectors which can convert incident light (ultraviolet, visible or infrared) into electrical signal are critical for a variety of industrial and scientific applications, including optical communications, environmental monitoring, day- and night-time surveillance and chemical/biological sensing.[1–4] Generally speaking, the photodetecors can be mainly devided into two type of sub-systems: special wavelength detector (ultraviolet detector, visible or infrared detector) and broadband detector, according to the wavelength range of operation. The special wavelength photodetectors are required under certain single wavelength light or the light with a narrow range, showing specific applications in light detecting and nano-optoelectronic integrated circuits. In comparison, the broadband photodetectors can detect the spectral ranges from ultraviolet to infrared and meet the demands on ultraviolet-visible light communication, wide spectral switches or memory storage through the use of single detector. During the light communication, in order to improve the transmission rate and increase the transmission capacity, the wide spectrum photodetection is necessary. In the case of ultraviolet-visible light communication, the photodetectors can be used in the sunlight and other illumination light which is in our daily lives. By utilizing the harmless characteristics of entire visible light, the visible photodetector is expected to be a promising candidate of high-power infrastructure for indoor/outdoor public ubiquitous data communication technology in the near future. So far, studies about photodetectors were mainly focused on their performances under special wavelength, due to the lack of proper materials which have the ability to absorb of incident radiation over broad wavelength range with excellent optoelectronic transfer efficiency. To expand the wavelength range of operation and obtain the enhanced properties, efforts have been devoted to design the photodetectors with wide spectral sensitivity through the combination of several different functional materials, which undergoes complicated fabrication process and requires expensive equipment (chemical vapor deposition, thermal evaporation, and so on), thus drawing back their applications. For example, the carbon nanotube/TiO_2 core-shell nanowires with broadband light-harvesting ability were grown through the atomic layer deposition (ALD) method by controlling the $TiCl_4/H_2O$ flow rate at 0.25 Å/cycles after preheated carbon nanotube in the ALD reactor chamber.[5] The expensive equipment and complicated fabrication processes will undoubtedly restrict their extensive applications. Thus, searching for proper materials with wide spectral sensitivity and easy assembly is urgently needed in the area of photodetectors.

Bearing this in mind, we paid our attention to the hybrid organolead halide perovskites with a general formula of $(RNH_3)MX_3$ (R = C_nH_{2n+1}; X = halogen I, Br, Cl; M = Pb, Cd, Sn and so on), which have attracted significant interests in electronic and photonic applications recently,[6–11] owing to their appropriate direct bandgap,[12] large absorption coefficient,[13] long range balanced electron and hole-transport lengths,[14,15] high electrical mobility,[16,17] and so on. Furthermore, the series of $(RNH_3)MX_3$ perovskites can be fabricated by a simple and cost-effective solution-based self-assembly method, rendering the $(RNH_3)MX_3$ to be a competitive candidate for the application

Dr. X. Hu, Dr. X. Zhang, Dr. L. Liang, Dr. J. Bao, Dr. S. Li, Dr. W. Yang, Prof. Y. Xie
Hefei National Laboratory for Physical Science at Microscale
Collaborative Innovation Center of Chemistry for Energy Materials
University of Science and Technology of China
Hefei, Anhui 230026, P. R. China
E-mail: zhxid@ustc.edu.cn; yxie@ustc.edu.cn

DOI: 10.1002/adfm.201402020

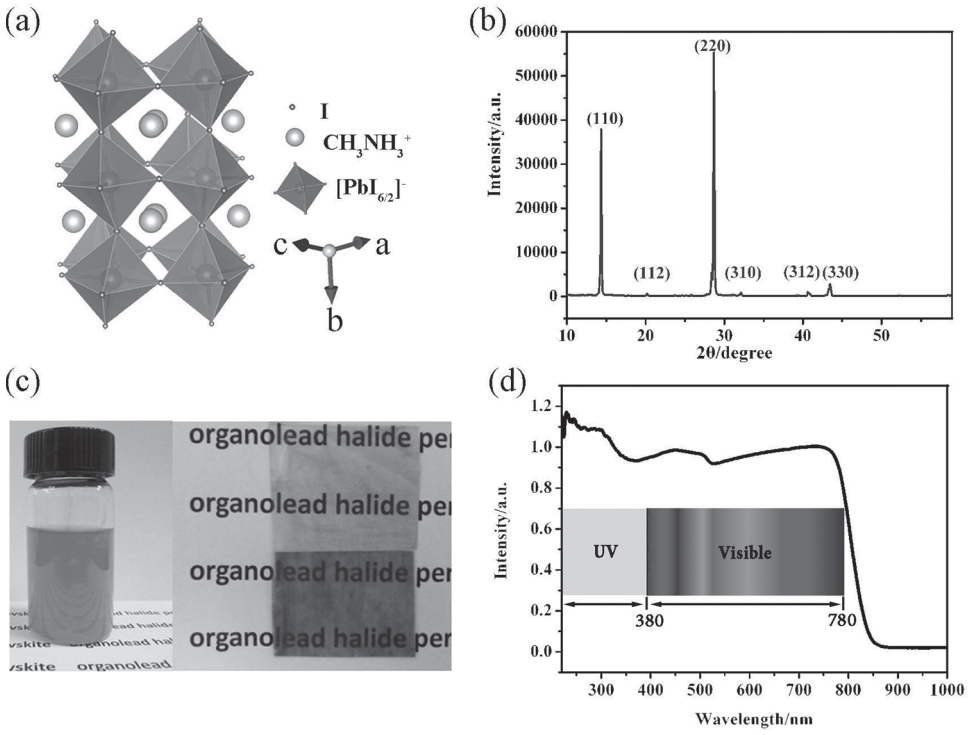

Figure 1. a) Three-dimensional schematic representation of perovskite structure of $CH_3NH_3PbI_3$. The image was produced using VESTA software.[41] b) XRD pattern of the $MAPbI_3$. c) The image of semitransparent $MAPbI_3$ thin films with different thickness. d) UV–Vis absorption spectrum of $MAPbI_3$ film.

in a plenty of electronic devices.[18] Despite extensive researches on the application of optical devices have been done,[12–15] studies on the design and fabrication of photodetector based on $(RNH_3)MX_3$ film have not been reported so far.

Herein, by depositing $CH_3NH_3PbI_3$ ($MAPbI_3$) film on flexible substrate, the first organolead halide perovskite based broadband photodetector is demonstrated. Because of the optimum bandgap and large absorption coefficient,[12] the $MAPbI_3$ can be sensitive to a wide spectra wavelength from ultraviolet to visible light, which is desirable for the design of broadband photodetector. In order to study the performance of $MAPbI_3$ film photodetector systematically, the spectrum of 365 nm and 780 nm are selected as representatives. The as-designed photodetectors have a high photo-to-dark current ratio, fast response speed, excellent stability and reproducibility. Our results not only demonstrate the uniqueness and effectiveness of $MAPbI_3$ for photodetection applications, but also provide a simple and low-cost method applicable for broadband light optical sensor production.

2. Results and Discussion

2.1. Synthesis and Structural Analysis

The $MAPbI_3$ has a distorted three-dimensional perovskite structure that crystallizes in the tetragonal *I4/mcm* space group at room temperature as schematically illustrated in **Figure 1**a.[19] The structure consists of lead cations in 6-fold coordination, surrounded by an octahedron of halide anions together with the organic components $(CH_3NH_3)^+$ in 12-fold cuboctahedral coordination. The significant hybridization between the Pb-6s and the I-5p states are formed in the polyhedron of $[PbI_{6/2}]^-$.[20] In this work, the $MAPbI_3$ film was prepared by drying 40 wt% of $MAPbI_3$/γ-butyrolactone solution in air at room temperature and was characterized by X-ray diffraction (XRD) and thermogravimetric analysis (TGA), as shown in Figures 1b and S1, respectively. The XRD of as-deposited film has two main peaks at 14.00° and 28.36°, which can be readily indexed to the (110) and (220) planes of the tetragonal perovskite structure (a = 8.855 Å and c = 12.659 Å).[21] The TGA spectrum shows that the perovskite crystal is thermally stable up to 300 °C, but quickly decomposes above this temperature due to the decomposition of the MAI component with a mass loss of 25.7%. The typical magnification SEM image of $MAPbI_3$ sample deposited on the flexible indium tin oxide (ITO)-coated polyethylene terephthalate (PET) sheet is shown in Figure S2a. The thin films with different thickness can be easily controlled by varying the volume of 20% $MAPbI_3$/γ-butyrolactone dilute solution, resulting in tunable and semitransparent film of $MAPbI_3$ (Figure 1c). In addition, the film of $MAPbI_3$ can also be easily formed on various rigid and flexible substrates, including Si, SiO_2, glass, PET and so on. As displayed in the UV–Vis absorption spectra of Figure 1d, the $MAPbI_3$ film shows a wide absorption spectrum, indicating high light-harvesting capabilities over the ultraviolet to visible spectrum.

As schematically illustrated in **Figure 2**a, the $MAPbI_3$ based photodetector was fabricated by depositing $MAPbI_3$ film on a flexible ITO/PET substrate with the bridging-gap width of about 15 μm and length of 1 cm, respectively. In order to

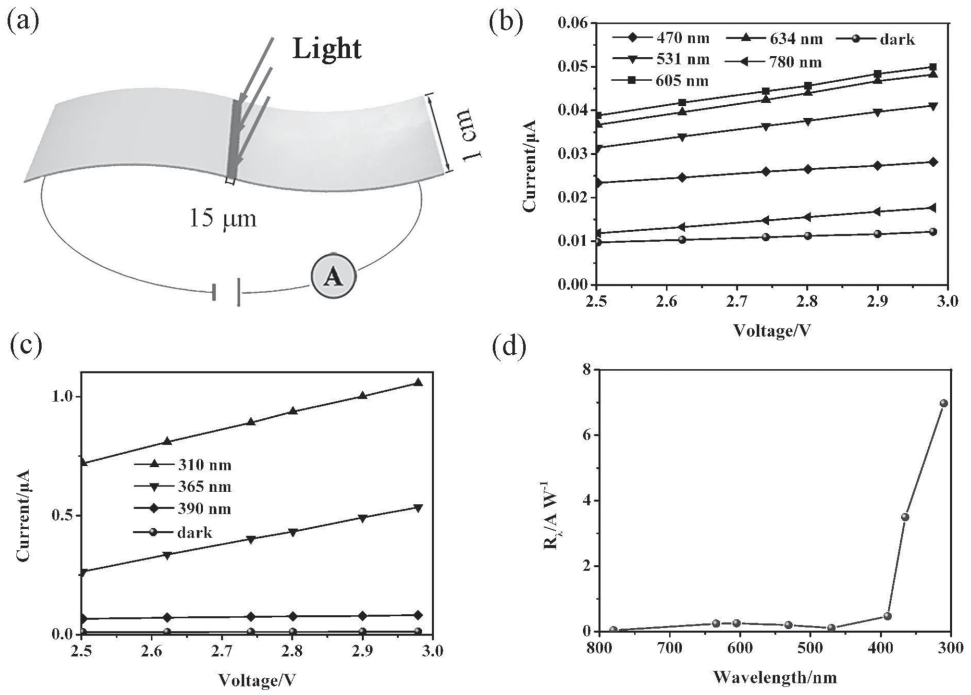

Figure 2. a) Schematic illustration of the $MAPbI_3$ film photodetector. b,c) Photocurrent response of the photodetector to monochromatic light in the ultraviolet and visible range. The light intensity is 0.01 mW cm^{-2}. d) Spectral photoresponse of $MAPbI_3$ film device at different wavelengths from 310 nm to 780 nm at a bias of 3V.

clearly illustrate the structure of the device, we have added the detailed schemes of the photodetector and the corresponding SEM images in Figure S3. The two adjacent ITO film is employed as conductive electrodes with the bridging $MAPbI_3$ film between them. The bridging-gap is filled with $MAPbI_3$ film and the thickness of the film is measured ca.1.5 μm (Figure S2b). The influence of ITO/PET substrate to the photoresponse has been excluded by the comparison experiments (Figure S4). To benchmark the performance of photodetector, two key criteria were measured: spectral responsivity ($R\lambda$) and external quantum efficiency (EQE). The spectral responsivity ($R\lambda$) can be defined as $R\lambda = \Delta I/PS$, where ΔI ($\Delta I = I_{photo} - I_{dark}$) is the difference between the photocurrent and dark current, P is the incident light intensity, and S is the effective illuminated area.[22] Figures 2b and 2c are the photocurrent response at different wavelengths from 310 to 780 nm (0.01 mW cm^{-2}) as a function of biasing voltage (applied across the film). The full I-V sweeps were shown in Figure S5. From the $MAPbI_3$ film device as shown in Figure 2a, based on the values of $\Delta I = 0.52283$ μA (Figure 2c) and S = 1.5×10^{-7} m^2, the $R\lambda$ of the photodetector irradiated by 365 nm light at 0.01 mW cm^{-2} is 3.49 A W^{-1}, under the bias voltage of 3 V. As shown in Figure 2d, the spectral photoresponse of the flexible photodetector clearly demonstrated the responsivities of this device range from 0.2 to 7.0 A W^{-1}, which are expected values of the light source and the monochromator from specifications, showing a broadband photodetection characteristic. The sharp increase of the spectral photoresponse below 400 nm, which is possibly attributed to the different concentration of the excited electron-hole pairs generating under various wavelength of lights. It is well known that the photoconduction is due to the electron-hole pairs excited by the incident light with energy larger than the band gap, only light with enough photon energy is able to induce a significant increase in conductance. Light with a larger energy in the short wavelength can excite more electrons from the valence band to the conduction band and thus contributes more to the photocurrent. The transition probability increases for higher photon energies, which is reflected in the monotonous increase of the photocurrent down to a 400 nm excitation wavelength.[23] For our device, the electrons have to overcome the Schottky barrier during transporting. Light with a larger energy in the short wavelength can excite more electrons from the valence band to the conduction band and thus contributes more to the photocurrent. As a result, the built-in potential of the Schottky barrier decreases, resulting in a large increase in free carrier density, leading to the easier carriers transport and tunnelling, thus, to a greatly enhanced photocurrent of the $MAPbI_3$ devices. It is worth noting that this is a common phenomenon in other broadband photodetectors, such as hybrid phenyl-C61-butyric acid methyl ester/Cd_3P_2 nanowire[24] with ultraviolet-visible-near infrared photodetecting ability, the monolayer MoS_2 photodetector with ultrasensitive broadband (< 680 nm),[23] the UV–Visible photodetector of atomically thin GaSe nanosheet[25] and the UV–Visible photodetector of ultrathin GaS nanosheet.[26] The broad photoresponse is also supported by the external quantum efficiency (EQE) spectrum. The EQE is defined as the number of electrons detected per incident photon and is expressed by the relationship: EQE = $hcR\lambda/e\lambda$, where h is Planck's constant, c is the velocity of light, e is the electronic charge and λ is the exciting wavelength.[27] In Figures 2b and 2c, the EQE of the $MAPbI_3$ film photodetector (at 3 V, 0.01 mW cm^{-2}) was calculated to be 1.19×10^3 % at 365 nm

and 5.84% at 780 nm, respectively. The performance data of $R\lambda$ and EQE of $MAPbI_3$ based photodetector are about 10^3 times higher than that of graphene (1×10^{-3} A W^{-1}, 6–16%),[28] graphene oxide (4×10^{-3} A W^{-1}, 0.3%)[29] and single-layer MoS_2 (7.5×10^{-3} A W^{-1}),[30] due to an efficient adsorption of photons for $MAPbI_3$. Nowadays, although some broadband photodetectors with nanowires and nanotubes have been demonstrated, their practical applications in high yield and scalable systems face formidable problems in assembly and manufacture. Materials with solution-based self-assembly can effectively avoid these limitations since they are compatible with established device designs and processing approaches in the semiconductor industry. All of these results demonstrate that the $MAPbI_3$ film can be used in highly sensitive photodetectors and fast photoelectric switches.

2.2. Flexible $MAPbI_3$ Film Photodetector Under 365 nm Light Illumination

To study the light response ability of the device, we explored its photosensitivity dependence on light intensity. As shown in **Figure 3**a, the current–voltage (I-V) curves of the device have been measured in the dark and under illumination with 365 nm light at different power intensities from 0.01 to 0.21 mW cm^{-2}. Under light illumination, the photocurrent of the devices increases drastically, particularly at high voltage bias, demonstrating a nonlinear and asymmetrical I-V behavior. The result indicates that a Schottky contact is formed. The Schottky contact might be attributed to the influence of the surface state (including surface defects, vacancies and adsorption) of the devices and the metal/semiconductor interface.[31] At the same voltage, the light current increases gradually with the increasing of light intensities, which can be attributed to a change in the photon intensity from the incident light. A high current of 0.26 μA was recorded at an applied voltage of 3 V when the device was illuminated with 365 nm light at a very low power intensity of 0.01 mW cm^{-2}, demonstrating the ultimate high sensitivity of the $MAPbI_3$ film photodetector. The intensity dependence of the photocurrent can be fitted by the power law $I \sim P^{0.44}$, where I is the photocurrent and P is the light intensity, as shown in Figure S6a. The photoswitching characteristic and stability of the flexible photodetector were investigated at room temperature in air. As shown in Figure S6b, the photocurrent as a function of time was measured during repetitive switching of 365 nm light illumination, under the alternative dark and illumination conditions at a different bias of 2, 3, 5 and 8 V, respectively. From the curves, it can be seen that the saturated photocurrent increases when the applied voltage is elevated at the identical light intensity. The photodetector, which could be reversibly and rapidly switched between the high and the low conductivity state as the light illumination, is periodically chopped at about 10 s interval, allowing the device to act as a high-quality photosensitive switch. At a higher bias of 8 V, the on/off current ratio can achieve around 20 with the photocurrent increases to 0.98 μA, while the dark current is only 0.05 μA. This value might become much larger when higher power irradiation is employed for the photocurrent measurement. Figure S7 shows the photocurrents of the devices during repeated switching of 365 nm light illumination at the bias of 1, 2, 5 and 8 V, respectively. The current of the photodetector reaches 17.50 μA under a high power irradiation of 0.13 mW cm^{-2}, producing a photocurrent on/off ratio of 324 with a bias of 8 V. A peak photoresponse current of 0.76 μA and an on/off current ratio of 152 can also be achieved, even at a lower bias of 1 V. The above results have shown that the $MAPbI_3$ photodetector can achieve high sensitivity and performance for a low-intensity optical signal. This is a particularly attractive attribute for low-power optoelectronic applications.

Repeatability and response speed are the key parameters to determine the capability of a photodetector. However, it is still a challenge to achieve photodetectors with both high repeatability and fast temporal response up to date. Figure 3b shows the photocurrent of the flexible devices during repetitive switching of light illumination, or on/off switching. No obvious degradation is detected for an average photocurrent of ~0.25 μA over 2000 s, indicating the excellent photocurrent stability of the $MAPbI_3$ based sensor. The inset of Figure 3b is the enlarged portion of 20–100 s range. For the application of photodetectors, a fast response and recovery speed are commonly desired characters. Herein, the rise time and decay time of the photodetector are defined as the time taken for the initial current to increase to 90% of the peak value, or vice versa. Figure 3c shows the more detailed transient photocurrent of this device from Figure 3b. The rise time and decay time are both shorter than 0.2 s. The high stability and fast response of the device are promising for large-area photodetector applications.

2.3. Flexible $MAPbI_3$ Film Photodetector Under 780 nm Light Illumination

Broad spectral detection is beneficial for extending the application range of photodetectors. To further study the broad-spectrum detection property of the perovskite photodetectors, the photoresponse characteristics of the flexible devices are studied under another wavelength of light (780 nm) from 0.2 to 4.5 mW cm^{-2}. Figure 3d shows typical current versus voltage plots of the device measured in the dark and under light illumination at different intensities. From the curves, it can be conspicuously seen that the current increases gradually with the increasing of light intensities when the same voltage is applied. The dependence relationship can be fitted with the power law as $I \sim P^{0.45}$ (Figure S8a). Time dependent photocurrent curves of the photodetector are also conducted by periodically turning a 780 nm light on and off at different applied voltages (2, 3, 5 or 8 V), as shown in Figure S8b. At a bias of 8 V, the dark current was 0.45 μA and when the flexible device was illuminated, the photocurrent increased to 15.20 μA, producing a photocurrent on/off ratio of 33. Even at a bias of 2.0 V, the on/off ratio achieves at 6.7 with the dark current and photocurrent of 0.25 μA and 1.69 μA, respectively. The value is larger than that of the photodetector illuminated by 365 nm light (Figure S6b) because of the larger light intensities, which also indicates the sensitive photoresponse characteristic of the flexible device. Figure 3e illustrates a photocurrent response of the device when 3 V bias voltage is applied with light intensity keeping at 0.2 mW cm^{-2} constantly. From the enlarged portion of typical on/off cycles

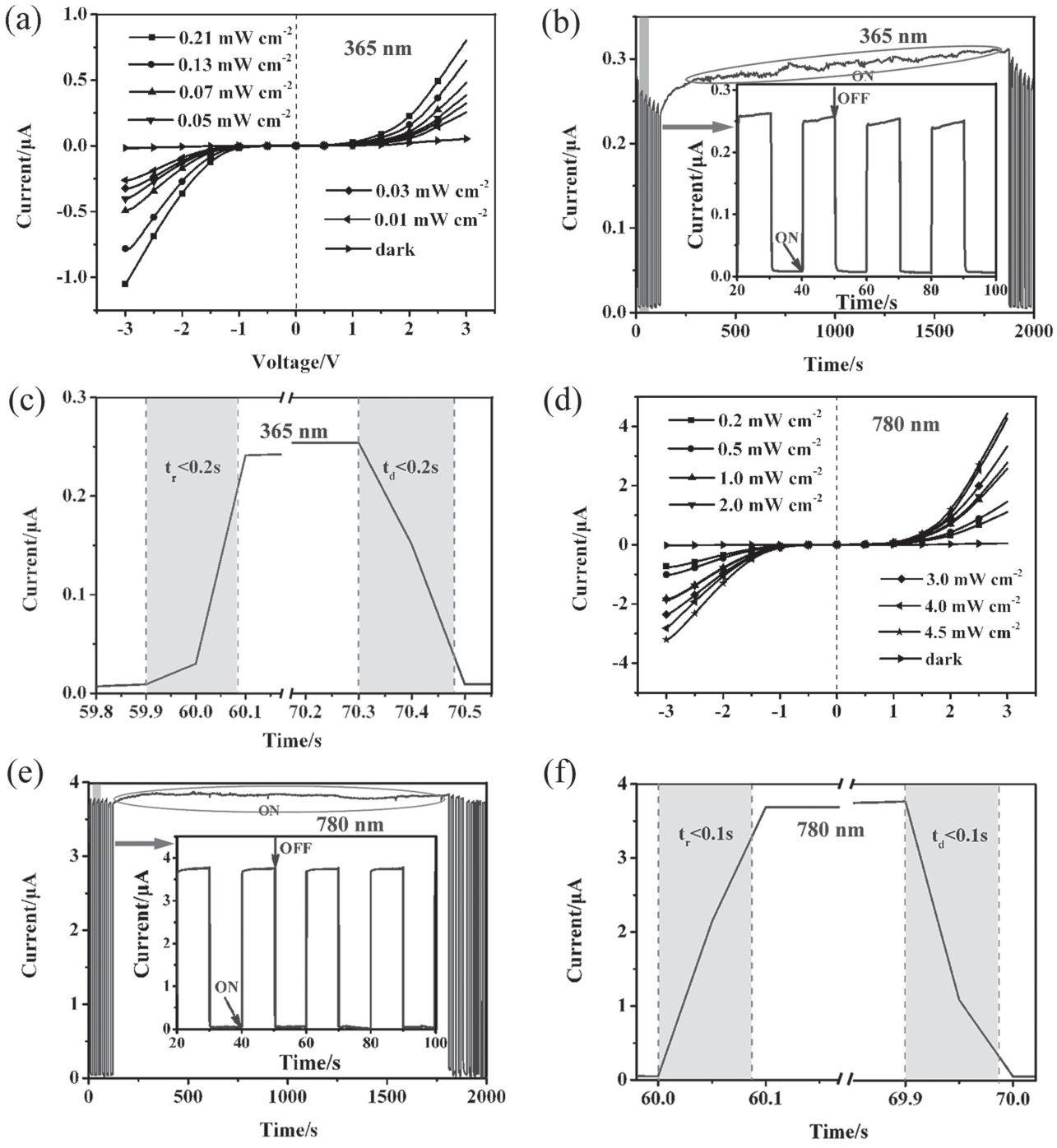

Figure 3. a,d) Photocurrent versus voltage plots of the device in the dark and under 365 nm, 780 nm light illumination at different intensities. b,e) A conductance response of the device upon 365 nm, 780 nm light illumination measured for light-on and light-off conditions at a 3 V applied voltage more than 30 min. The enlarged portions of a 20–100 s range from the highlighted part in (b) and (e), respectively. c,f) Photocurrent rise and decay of the device measured at a bias of 3 V and at a light intensity of 0.01 mW cm^{-2},0.2 mW cm^{-2} for 365 nm, 780 nm, respectively.

in Figure 3f, it can be seen that both of the rise time and decay time are shorter than 0.1 s, which are quite outstanding values in light of previously reported flexible detectors. For example, a ZnOEP nanowire-based white light photodetector possesses the rise time of 0.9 s and the decay time of 1.7 s.[32] The photocurrent rise and decay time of Zn_3As_2 NW-array device on PET substrate are 0.14 s and 2.9 s,[33] respectively. As one of the key factors for detection performance, the relatively faster response time can naturally broaden the scope of the device applications. The above results indicate that the $MAPbI_3$ device on the flexible substrate has an excellent stability, reproducibility, and fast detection time, demonstrating that the device should

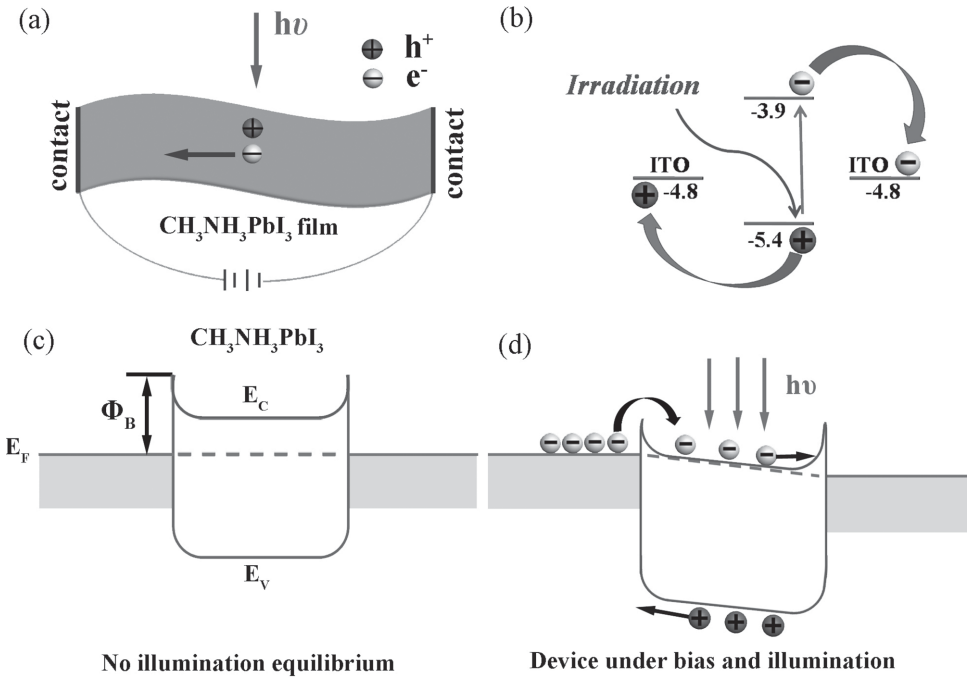

Figure 4. a) Schematic of the $MAPbI_3$ photoconductor. Upon illumination with photon energy above E_g, electron-hole pairs are generated. b) Energy level diagram of the corresponding materials used in our devices. c) Band diagram of the $MAPbI_3$ photodetector, taking into consideration Schottky barriers at the contacts. E_F, E_C and E_V are the Fermi level energy, conduction band energy, valence band energy, respectively. Φ_B is the Schottky barrier height. There is no electrical current flowing under equilibrium conditions and no illumination. d) Under light illumination, Schottky barriers is lower lead to photogenerated holes migrate to the surface and are trapped, leaving behind unpaired electrons in the $MAPbI_3$ that contribute to the photocurrent, resulting in a more efficient photocurrent extraction and increased photoresponse.

be suited for the application in optoelectronic switches and photodetectors.

The photoresponse property of the device was proposed to relate to the Schottky barrier owing to the non-symmetrical I-V curves. During the study of photoresponse mechanisms, the hole-trapping mechanism based on the existence of chemisorbed oxygen molecules at surfaces is considered to dominant in an inorganic semiconductor.[34] Considering that the studies of the $MAPbI_3$ film photodetector were performed in air and the device is exposed in oxygen atmosphere, the existence of the oxygen chemisorption/desorption effect should be excluded. Taking 365 nm as an instance, the I-V curves and the time dependent photocurrent curves of the same device have been measured in air and in vacuum at a bias of 3 V. As illustrated in Figure S9, the photocurrents in air and in vacuum remain almost unchanged, revealing the insensitivity of photocurrent to oxygen molecules. This means that the oxygen molecules do not change the film's conductance. Therefore, a different conducting mechanism for the $MAPbI_3$ film device is proposed. The observed behavior of our photodetector can be explained by a simple energy band diagram (**Figure 4**). Without illumination and bias voltage, the device is in its equilibrium state, characterized by Schottky barriers at the contacts between the ITO electrodes and the $MAPbI_3$ film or the internal $MAPbI_3$ film, as shown in Figure 4c. The electrons have to overcome the Schottky barrier during transporting. Upon illumination, with a photoenergy larger than that of the semiconductor band gap (E_g), the $MAPbI_3$ film absorbs photons to generate a large number of electron-hole pairs [$h\nu \rightarrow e^- + h^+$]. The local electric field at the reversely biased Schottky barrier area not only separate the photogenerated electrons and holes quickly but also reduce the electron-hole recombination rates, resulting in an increase in free carrier density.[35] The increased carrier density in $MAPbI_3$ film upon illumination lowers the effective barrier height, leading to the easier carriers tunnelling and carrier transport, thus, to a significant enhancement in conductivity. It is worth noting that the reversely biased Schottky barrier induced excitons dissociation has been found in a variety of photodetectors, such as a Schottky-contact ZnO nanowire photodetectors[35,36] and monolayer MoS_2 photodetectors.[37]

On the other hand, considering the structure of the device, when ITO electrodes and $MAPbI_3$ film are contacted, a charge transfer occurs at the interfaces via Femi level tuning under an equilibrium condition, which will cause the accumulation of space charge in the contact region together with band bending to form a Schottky-type barrier as well as a depletion layer near the surface of the $MAPbI_3$ film. And the depletion layer assists in the charge separation.[38] Both of the above reasons account for the improved separation of the photogenerated excitons. After the excitons dissociation, electrons would inject into the conduction band of $MAPbI_3$ and further to the ITO cathode, while the holes would travel to the valence bands of $MAPbI_3$ and the ITO anode (Figure 4b), where the $MAPbI_3$ was played as a double roles for light harvester and hole conductor.[38–40] When the light illumination is turned off, the carrier recombination will result in a significant increase in the Schottky barrier height due to the greatly reduced carrier density.

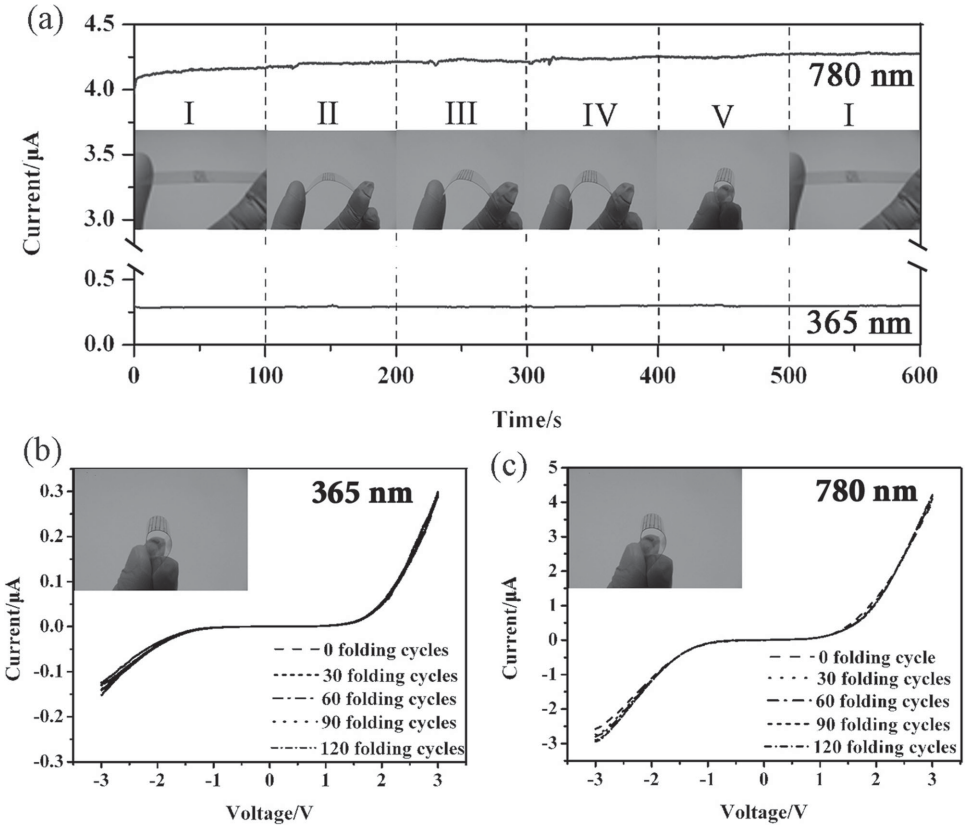

Figure 5. a) The I-t curves of the flexible hybrid photodetector when bent with different curvatures under a bias voltage of 3.0 V at the light intensity of 0.01, 0.2 mW cm^{-2} for 365 nm, 780 nm, respectively. The inserts are corresponding photographs of the device under the different bending states. b,c) I-V curves of the flexible photodetector under 365 nm, 780 nm light illumination without bending and after 30, 60, 90 and 120 cycles of bending.

In order to apply for practical applications, the stable electrical properties of the flexible device under bending should be investigated. Bearing this in mind that, we further studied the electrical stability of the flexible $MAPbI_3$ based photodetector at various bending curvatures as shown in the insets of **Figure 5**a. In the bending process, five different bending states of the flexible device were studied and labelled as state I, II, III, IV, and V, respectively. As shown in Figure 5a, the photocurrents through the flexible device remained nearly unchanged at a fixed voltage of 3 V at five different states, revealing that the photocurrents of the flexible device would not be influenced by external bending stress under both of the 365 nm and 780 nm light illumination. In order to accommodate flexible electrical devices, the electrical properties of the device should remain unchanged after bending. The plots in Figure 5b and 5c are the I-V curves of the device before and after bending for different cycles, respectively. From the curves, it can be seen clearly that the conductance of $MAPbI_3$ film remains almost constant even after 120 cycles of bending. These results indicate the extreme flexibility, good folding endurance and electrical stability of the flexible device.

3. Conclusion

In summary, the first organolead halide perovskites photodetectors based on $MAPbI_3$ film were fabricated through a low-cost, solution-processed and self-assembly strategy on flexible substrates. In the photocurrent measurement, the photodetector has a broad photoresponse range from 780 nm to 310 nm, far exceeding the performance of current photodetectors. Besides, the photodetector was characterized in terms of power intensity dependent photoresponse and time-resolved photocurrent. The photoresponse and external quantum efficiency of the $MAPbI_3$ film-based flexible photodetectors were measured at different wavelengths and reached 3.49 AW^{-1}, 1.19×10^3 %, respectively, at 365 nm. This demonstrates that the photodetector shows high sensitivity, fast response speed and excellent stability, indicating that the developed $MAPbI_3$ film photodetector is a great candidate for applications in broadband light detection, and may be further extended to applications in optoelectronic devices.

4. Experimental Section

Synthesis and Characterization of $CH_3NH_3PbI_3$: The ethylammonium lead iodide ($CH_3NH_3PbI_3$) perovskite was prepared as reported elsewhere.[5,6] Methylamine (CH_3NH_2) (13.5 mL, 40 wt% in aqueous solution, Alfa Aesar) and hydroiodic acid (HI) (15.0 mL, 57 wt% in water, Alfa Aesar) were stirred at 0°C under nitrogen atmosphere for 2 h. After the reaction, the solvent of the solution was evaporated using a rotary evaporator. A white powder, methyl ammonium iodide (CH_3NH_3I), was generated by the reaction. The precipitate was washed with diethyl

ether (Sigma-Aldrich) three times and dried at 60°C in a vacuum oven overnight. $CH_3NH_3PbI_3$ was synthesized by mixing CH_3NH_3I and lead iodide (PbI_2) (Aldrich) at 1:1 (0.8 : 2.3 g) equimolar ratio in γ-butyrolactone (Aldrich) (15.8 mL, 14.9 wt% solution) (17.2 wt% solution) at 60 °C, stirring for 12 h inside a nitrogen-filled glove box with oxygen and moisture levels < 1 ppm. The concentration of $CH_3NH_3PbI_3$ was 40 wt%. The samples were characterized by X-ray powder diffraction (XRD) by a Philips XQPert Pro Super diffractometer equipped with graphite-monochromatized Cu-Kα radiation (λ = 1.54178 Å). UV–Vis–NIR absorption spectrum was recorded on a Perkin Elmer Lambda 950 UV/Vis–NIR spectrophotometer.

Fabrication of the Flexible Photodetectors: Flexible photoresponse devices were fabricated by drop-casting of the solution with 40 wt% of $MAPbI_3$/γ-butyrolactone solution onto the pre-cleaned flexible ITO electrodes at a rate of 500 rpm and dried in air naturally.

Photoresponse Measurements: Electric and optoelectronic measurements of the fabricated devices were performed in a three-electrode system on an electrochemical workstation (CHI660B). The different wavelength (310 nm to 634 nm) lights from a 300 W Xe lamp were focused through a monochromator. The 780 nm light source was monochromatic light (100 mW). The incident power light was measured power meter. All measurements were performed in air and at room temperature.

Supporting Information

Supporting Information is available from the Wiley Online Library or from the author.

Acknowledgements

The research was financially supported by National Natural Science Foundation of China (11079004, 21331005, 11321503), Chinese Academy of Science (XDB01020300), and Fundamental Research Funds for the Central University (WK2060190032).

Received: June 19, 2014
Revised: August 21, 2014
Published online: September 11, 2014

[1] J. J. Wang, F. F. Cao, L. Jiang, Y. G. Guo, W. P. Hu, L. J. Wan, *J. Am. Chem. Soc.* **2009**, *131*, 15602.
[2] H. Kind, H. Yan, B. Messer, M. Law, P. Yan, *Adv. Mater.* **2002**, *14*, 158.
[3] J. S. Jie, W. J. Zhang, Y. Jiang, X. M. Meng, Y. Q. Li, S. T. Lee, *Nano Lett.* **2006**, *6*, 1887.
[4] T. B. Yang, K. Sun, X. L Liu, W. Wei, T. Z. Yu, X. Gong, D. L. Wang, Y. Cao, *J. Phys. Chem. C* **2012**, *116*, 13650.
[5] C. Y. Hsu, D. H. Lien, S. Y. Lu, C. Y. Chen, C. F. Kang, Y. L. Chueh, W. K. Hsu, J. H. He, *ACS Nano* **2012**, *6*, 6687.
[6] D. B. Mitzi, C. A. Feild, W. T. A. Harrison, A. M. Guloy, *Nature* **1994**, *369*, 467.
[7] D. B. Mitzi, S. Wang, C. A. Feild, C. A. Chess, A. M. Guloy, *Science* **1995**, *267*, 1473.
[8] D. B. Mitzi, *Chem. Mater.* **1996**, *8*, 791.
[9] S. Zhang, P. Audebert, Y. Wei, J. S. Lauret, L. Galmiche, E. Deleporte, *J. Mater. Chem.* **2011**, *21*, 466.
[10] N. Kitazawa, Y. Watanabe, *J. Phys. Chem. Solids* **2010**, *71*, 797.
[11] Z. Y. Cheng, B. X. Gao, M. L. Pang, S. Y. Wang, Y. C. Han, J. Lin, *Chem. Mater.* **2003**, *15*, 4705.
[12] J. Y. Jeng, Y. F. Chiang, M. H. Lee, S. R. Peng, T. F. Guo, P. Chen, T. C. Wen, *Adv. Mater.* **2013**, *25*, 3727.
[13] M. M. Lee, J. Teuscher, T. Miyasaka, T. N. Murakami, H. J. Snaith, *Science* **2012**, *338*, 643.
[14] S. D. Stranks, G. E. Eperon, G. Grancini, C. Menelaou, M. J. P. Alcocer, T. Leijtens, L. M. Herz, A. Petrozza, H. J. Snaith, *Science* **2013**, *342*, 341.
[15] G. C. Xing, N. Mathews, S. Y Sun, S. S. Lim, Y. M. Lam, M. Grätzel, S. Mhaisalkar, T. C. Sum, *Science* **2013**, *342*, 344.
[16] C. C. Stoumpos, C. D. Malliakas, M. G. Kanatzidis, *Inorg. Chem.* **2013**, *52*, 9019.
[17] G. Hodes, *Science* **2013**, *342*, 317.
[18] J. Burschka, N. Pellet, S. J. Moon1, R. Humphry-Baker, P. Gao, M. K. Nazeeruddin, M. Grätzel, *Nature* **2013**, *499*, 316.
[19] A. Poglitsch, D. Weber, *J. Chem. Phys.* **1987**, *87*, 6373.
[20] M. H. Du, *J. Mater. Chem. A.* **2014**, *2*, 9091.
[21] J. H. Heo, S. H. Im, J. H. Noh, T. N. Mandal, C. S. Lim, J. A. Chang, Y. H. Lee, H. J. Kim, A. Sarkar, M. K. Nazeeruddin, M. Grätzel, S. II Seok, *Nat. Photonics* **2013**, *7*, 486.
[22] L. Li, P. C. Wu, X. S. Fang, T. Y. Zhai, L. Dai, M. Y. Liao, Y. Koide, H. Q. Wang, Y. Bando, D. Golberg, *Adv. Mater.* **2010**, *22*, 3161.
[23] O. Lopez-Sanchez, D. Lembke, M. Kayci, A. Radenovic, A. Kis, *Nat. Nanotech.* **2013**, *8*, 497.
[24] G. Chen, B. Liang, X. Liu, Z. Liu, G. Yu, X. M. Xie, T. Luo, D. Chen, M. Q. Zhu, G. Z. Shen, Z. Y. Fan, *ACS Nano* **2014**, *8*, 787.
[25] P. A. Hu, Z. Z. Wen, L. F. Wang, P. H. Tan, K. Xiao, *ACS Nano* **2012**, *6*, 5988.
[26] P. A. Hu, L. F. Wang, M. Yoon, J. Zhang, W. Feng, X. N. Wang, Z. Z. Wen, J. C. Idrobo, Y. Miyamoto, D. B. Geohegan, K. Xiao, *Nano Lett.* **2013**, *13*, 1649.
[27] T. Y. Zhai, X. S. Fang, M. Y. Liao, X. J. Xu, L. Li, B. D. Liu, Y. S. Koide, Y. Ma, J. N. Yao, Y. Bando, D. Golberg, *ACS Nano* **2010**, *4*, 1596.
[28] T. Mueller, F. Xia, P. Avouris, *Nat. Photonics* **2010**, *4*, 297.
[29] B. Chitara, L. S. Panchakarla, S. B. Krupanidhi, C. N. R. Rao, *Adv. Mater.* **2011**, *23*, 5419.
[30] Z. Yin, H. Li, H. Li, L. Jiang, Y. Shi, Y. Sun, G. Lu, Q. Zhang, X. Chen, H. Zhang, *ACS Nano* **2012**, *6*, 74.
[31] H. Kind, H. Yan, B. Messer, M. Law, P. Yang, *Adv. Mater.* **2002**, *14*, 158.
[32] F. X. Wang, J. Lin, W. B. Gu, Y. Q. Liu, H. D. Wu, G. B. Pan, *Chem. Commun.* **2013**, *49*, 2433.
[33] G. Chen, Z. Liu, B. Liang, G. Yu, Z. Xie, H. T. Huang, B. Liu, X. F. Wang, D. Chen, M. Q. Zhu, G. Z. Shen, *Adv. Funct. Mater.* **2013**, *23*, 2681.
[34] T. Y Zhai, L. Li, X. Wang, X. S. Fang, Y. Bando, D. Golberg, *Adv. Funct. Mater.* **2010**, *20*, 4233.
[35] Y. F. Hu, J. Zhou, P. H. Yeh, Z. Li, T. Y. Wei, Z. L. Wang, *Adv. Mater.* **2010**, *22*, 3327.
[36] J. Zhou, Y. D. Gu, Y. F. Hu, W. J. Mai, P. H. Yeh, G. Bao, A. K. Sood, D. L. Polla, Z. L. Wang, *Appl. Phys. Lett.* **2009**, *94*, 191103.
[37] O. Lopez-Sanchez, D. Lembke, M. Kayci, A. Radenovic, A. Kis, *Nat. Nanotech.* **2009**, *4*, 839.
[38] S. Aharon, S. Gamliel, B. E. Cohen, L. Etgar, *Phys. Chem. Chem. Phys.* **2014**, *16*, 10512.
[39] L. Etgar, P. Gao, Z. S. Xue, Q. Peng, A. K. Chandiran, B. Liu, M. K. Nazeeruddin, M. Grätzel, *J. Am. Chem. Soc.* **2012**, *134*, 17396.
[40] J. J Shi, J. Dong, S. Lv, Y. Z. Xu, L. F. Zhu, J. Y. Xiao, X. Xu, H. J. Wu, D. M. Li, Y. H. Luo, Q. B. Meng, *Appl. Phys. Lett.* **2014**, *104*, 063901.
[41] K. Momma, F. Izumi, *J. Appl. Crystallogr.* **2008**, *41*, 653.